Deterministic Steering of Quantum Trajectories in the Generalized Rate Operator Formalism

Master's Thesis
University of Turku
Theoretical Physics
2026
B.Sc. Tiia Salokorpi
Examiners:
Prof. Jyrki Piilo
Doc. Iiro Vilja

In accordance with the quality assurance system of the University of Turku, the originality of this publication has been checked using the Turnitin OriginalityCheck system.

TURUN YLIOPISTO
Department of Physics and Astronomy

Student, Tiia Salokorpi Deterministic Steering of Quantum Trajectories in the Generalized Rate Operator Formalism

Master's Thesis, 38 pp.
Theoretical Physics
June 2026

This thesis studies realization-dependent transformations in the generalized rate-operator quantum-jump formalism for open quantum systems. The aim is to examine whether these transformations can be used to steer the deterministic part of individual quantum trajectories toward a prescribed fixed target state, while preserving the physicality of the stochastic trajectories. This question is motivated by state-preparation tasks, where a quantum system must be driven to a known state quickly and with high probability, as in qubit resetting, qubit initialization, and the preparation of resourceful states.

The theoretical part of the thesis introduces the basic framework of quantum mechanics, open quantum system dynamics, master equations, and stochastic quantum trajectories. The numerical part focuses on qubit dynamics and compares two examples: pure dephasing dynamics and Pauli master equation dynamics. For each fixed transformation, the simulations check the positivity condition, the attraction toward the target state, and the survival probability of the deterministic no-jump evolution.

The results show that the simple fixed transformation considered for pure dephasing does not provide simultaneous attraction and positivity. In contrast, for Pauli master equation dynamics, fixed transformations are found that steer the deterministic trajectory toward the target while keeping the generalized rate operator positive. Because the isotropic Pauli master equation treats all directions on the Bloch sphere equally, the specific choice of the target state is just a reference direction, and the result carries over to any pure target state by symmetry. The survival probability analysis shows that steering can be achieved with quite high no-jump probability for the suitable parameter choices. The results suggest that realization-dependent transformations can provide useful trajectory level control in suitable open system dynamics.

Keywords: open quantum systems, non-Markovian dynamics, quantum jumps, stochastic unravelings, rate operator

Contents

Introduction

No real quantum system is perfectly isolated from its surroundings. Interactions with the environment introduce effects like dissipation, decoherence, and the gradual loss of information from the system to its surroundings. The theory of open quantum systems deals with exactly this situation by focusing on the reduced state of the system rather than tracking the full system-environment state. The evolution is then typically described by a quantum master equation for the density operator [1].

The Markovian approximation assumes that the environment has no relevant memory of the system, which simplifies the description considerably. In many situations this approximation works well enough, but this is not always the case. In non-Markovian dynamics, memory effects can feed back into the later evolution of the system in ways that the Markovian picture misses entirely. These effects show up in questions about information flow, the divisibility of dynamical maps, and whether time-local master equations with temporarily negative decay rates can still be physically valid [2].

Quantum trajectory methods offer a different angle on open-system dynamics. Rather than working only with the density matrix, the evolution can be written as an ensemble average over stochastic pure-state trajectories. In quantum-jump approaches, the state evolves deterministically between sudden jumps, which makes the connection between master equations, stochastic processes, and individual realizations much more concrete. It also turns out to be a practically useful framework for numerical work [3].

This thesis focuses on the generalized rate-operator quantum-jump formalism with realization-dependent transformations. The key idea is that different stochastic unravelings can correspond to the same master equation, while the transformation modifies the deterministic part of each individual trajectory. The question studied here is whether this freedom can be used to steer deterministic trajectories toward a

chosen target state, without violating the positivity of the generalized rate operator. Positivity matters because the eigenvalues of the rate operator determine the jump probabilities and cannot be negative. The problem is studied for qubit dynamics, with particular attention to pure dephasing and Pauli master equation dynamics [4].

1 Foundations of quantum mechanics

1.1 Hilbert space formulation

The pure states of a quantum system are represented by a vector $|\psi\rangle$ in the Hilbert space. Pure states are normalized, so

$$\langle\psi|\psi\rangle = 1. \tag{1}$$

Since the inner product defines orthogonality, one can construct an orthonormal basis $\{|\phi_i\rangle\}$ satisfying $\langle\phi_i|\phi_j\rangle = \delta_{ij}$. Any state of the system can then be written as a linear combination of the basis states

$$|\psi\rangle = \sum_i c_i|\phi_i\rangle, \tag{2}$$

where the coefficients c_i are complex numbers. The basis states also define the identity operator through the completeness relation $I = \sum_i |\phi_i\rangle\langle\phi_i|$.

Physical observables are represented by linear operators acting on the Hilbert space. If $A = A^\dagger$ is an observable, its eigenvalues and eigenvectors satisfy

$$A|\phi_n\rangle = a_n|\phi_n\rangle. \tag{3}$$

where the eigenvalues a_n are real, and the eigenvectors ϕ_n can be chosen to be mutually orthogonal.

The expectation value of an observable A in the state $|\psi\rangle$ is given by

$$\langle A\rangle = \langle\psi|A|\psi\rangle. \tag{4}$$

and this relation connects the mathematical description of the state with measurable physical quantities [5].

1.2 Density matrices

The Hilbert-space description in terms of state vectors is sufficient for pure states, but in many physical situations a more general formulation is needed. The system may be entangled with another system, or only statistical information about its preparation may be available. In such cases, the state cannot be described by a single state vector. Instead, it is described as a mixed state, which is written as a convex combination of pure states.

For a pure state $|\psi\rangle$, the corresponding projector operator is

$$P_\psi = |\psi\rangle\langle\psi|. \tag{5}$$

For mixed states, the state-vector description is replaced by the density-operator formalism. If the system is prepared in the pure state $|\psi_i\rangle$ with probability p_i, the corresponding mixed state is described by a density operator

$$\rho = \sum_i p_i |\psi_i\rangle\langle\psi_i|, \tag{6}$$

where the probabilities satisfy the normalization condition $\sum_i p_i = 1$, $p_i \geq 0$. The density operator contains the complete statistical description of the quantum system.

In a chosen basis, the diagonal elements of the density matrix ρ_{ii} represent the populations, that is, the probabilities of finding the system in the corresponding basis states. The off-diagonal elements $\rho_{ij}, i \neq j$, describe the coherences between different basis states. The density matrix gives a more general description than a state vector and is especially useful when discussing mixed states and open quantum systems. The density operator has several important properties: it is Hermitian, positive, and has unit trace

$$\rho^\dagger = \rho, \qquad \rho \geq 0, \qquad \mathrm{Tr}(\rho) = 1. \tag{7}$$

These properties imply that the eigenvalues of ρ are non-negative and sum to one. Therefore, they form a probability distribution, in agreement with the spectral decomposition of the density operator.

A pure state is a special case of the density matrix description, and the density matrix satisfies the condition

$$\rho^2 = \rho. \tag{8}$$

This property can also be expressed in terms of the purity of the state, which is defined as the trace of the squared density operator. For mixed states, purity is smaller than one

$$\mathrm{Tr}(\rho^2) < 1. \tag{9}$$

and for a pure state the purity is one.

The expectation value of an observable A can also be written in terms of the density matrix. If A is an observable represented by a Hermitian operator, the expectation value in the state ρ is given by

$$\langle A \rangle = \mathrm{Tr}(\rho A). \tag{10}$$

This expression is valid for both pure and mixed states and generalizes the expectation value formula of the Hilbert space formulation [1, 5].

1.3 Qubit systems and Bloch sphere

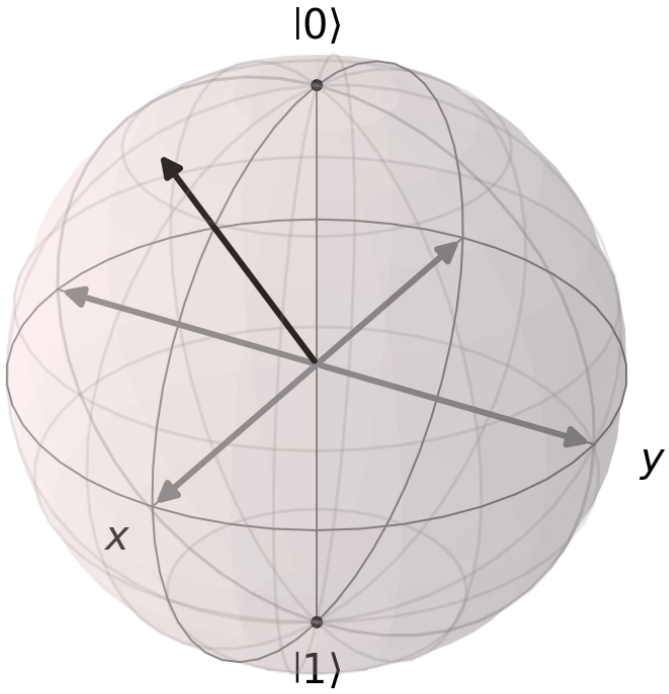

Figure 1. Bloch sphere representation of a qubit state. Pure states lie on the surface of the sphere, while mixed states correspond to points inside the sphere. The black arrow denotes the Bloch vector **r** that specifies the state of the system.

The simplest nontrivial quantum system is a two-level quantum system, commonly referred to as a qubit. A qubit can be realized in several physical systems, such as the spin of an electron, the polarization of a photon, or two internal energy levels of an atom. Mathematically, the state space of a qubit is the two-dimensional Hilbert space $\mathbb{C}^2$.

A convenient orthonormal basis for this space is

$$|0\rangle = \begin{pmatrix} 1 \\ 0 \end{pmatrix}, \qquad |1\rangle = \begin{pmatrix} 0 \\ 1 \end{pmatrix}. \tag{11}$$

and an arbitrary pure state of a qubit can then be written as a linear combination

of these basis states

$$|\psi\rangle = \alpha|0\rangle + \beta|1\rangle, \tag{12}$$

where α and β are complex coefficients satisfying the normalization condition

$$|\alpha|^2 + |\beta|^2 = 1. \tag{13}$$

Since an overall global phase has no physical significance, the state of a qubit can be parametrized using two real parameters. A common parametrization is

$$|\psi\rangle = \cos\left(\frac{\theta}{2}\right)|0\rangle + e^{i\phi}\sin\left(\frac{\theta}{2}\right)|1\rangle, \tag{14}$$

where $0 \leq \theta \leq \pi$ and $0 \leq \phi < 2\pi$. This parametrization provides a geometric representation of qubit states known as the Bloch sphere.

In this representation, each pure state corresponds to a point on the surface of a unit sphere whose cartesian coordinates are given by

$$x = \sin\theta\cos\phi, \tag{15}$$

$$y = \sin\theta\sin\phi, \tag{16}$$

$$z = \cos\theta. \tag{17}$$

The state of a qubit can be described by the density matrix

$$\rho = \frac{1}{2}\left(I + \mathbf{r}\cdot\boldsymbol{\sigma}\right), \tag{18}$$

where $\mathbf{r} = (r_x, r_y, r_z)$ is the Bloch vector, with components

$$r_i = \mathrm{Tr}(\rho\,\sigma_i), \qquad i = x, y, z, \tag{19}$$

satisfying $|\mathbf{r}| \leq 1$. I represents the identity operator and $\boldsymbol{\sigma} = (\sigma_x, \sigma_y, \sigma_z)$ are the Pauli matrices. Pure states correspond to $|\mathbf{r}| = 1$ and lie on the surface of the Bloch sphere, whereas mixed states correspond to $|\mathbf{r}| < 1$ and lie inside the sphere, as shown in Figure 1 [6].

1.4 Quantum evolution

The time evolution of an isolated quantum system is unitary. If the system is initially in the state $|\psi(0)\rangle$, then the state at time t is

$$|\psi(t)\rangle = U(t)|\psi(0)\rangle. \tag{20}$$

where the operator $U(t)$ forms a one-parameter family of unitary transformations that describe the continuous time evolution of the quantum state [6].

The unitary time evolution of the quantum state is generated by the Schrödinger equation. For a state vector $|\psi(t)\rangle$ the equation of motion is given by

$$i\hbar\frac{d}{dt}|\psi(t)\rangle = H(t)|\psi(t)\rangle, \tag{21}$$

where H is the Hamiltonian operator of the system. For a time-independent Hamiltonian, the unitary evolution operator can be written in the exponential form

$$U(t) = e^{-iHt/\hbar}. \tag{22}$$

thus the Hamiltonian operator acts as the generator of the unitary time evolution of the quantum state [5].

The time evolution can also be expressed in terms of the density matrix formalism introduced earlier. If the initial state of the system is described by the density operator $\rho(0)$, the state at time t evolves according to

$$\rho(t) = U(t)\rho(0)U^{\dagger}(t). \tag{23}$$

Differentiating this expression with respect to time and using the Schrödinger equation leads to the Liouville–von Neumann equation

$$\frac{d\rho}{dt} = -\frac{i}{\hbar}[H, \rho], \tag{24}$$

which is the equation of motion for the density operator of a closed system [1].

2 Open quantum system dynamics

No real quantum system is perfectly isolated from its surroundings. Interaction with the environment introduces irreversible effects, such as dissipation and decoherence, that cannot be captured by the unitary evolution.

The theory of open quantum systems focuses on the system of interest alone, tracing out the environmental degrees of freedom to obtain a reduced description. The resulting equation of motion for the reduced density operator is called a master equation, and it forms the central framework of open quantum system dynamics [1].

2.1 System–environment interaction

To describe an open quantum system, one considers a total Hilbert space of the system and environment

$$\mathcal{H} = \mathcal{H}_S \otimes \mathcal{H}_E, \tag{25}$$

where $\mathcal{H}_S$ and $\mathcal{H}_E$ are the Hilbert spaces of the system and environment respectively. Since the combined system is closed, its evolution remains unitary, governed by the Hamiltonian

$$H(t) = H_S(t) \otimes I_E + I_S \otimes H_E(t) + H_I(t), \tag{26}$$

where $H_S(t)$ is the Hamiltonian of the system, $H_E(t)$ is the Hamiltonian of the environment, and $H_I(t)$ describes the interaction between them [1].

2.1.1 Reduced dynamics

Since all observables of interest act only on the system, the relevant state is the reduced density operator

$$\rho_S = \mathrm{Tr}_E(\rho), \tag{27}$$

where ρ is the density operator of the total system and Tr_E denotes the partial trace over the environmental degrees of freedom. Expectation values of system observables are then computed as

$$\langle A \rangle = \mathrm{Tr}_S(A\rho_S), \tag{28}$$

where A is an observable acting on the system's Hilbert space [1].

If the total system evolves unitarily with the operator $U(t)$, the reduced density operator at time t is

$$\rho_S(t) = \mathrm{Tr}_E\left[U(t)\rho(0)U^\dagger(t)\right]. \tag{29}$$

Differentiating this expression with respect to time and taking the partial trace over the environment yields the exact equation of motion

$$\frac{d\rho_S(t)}{dt} = -\frac{i}{\hbar}\mathrm{Tr}_E([H(t), \rho(t)]). \tag{30}$$

Although this equation is exact, it is generally not closed in terms of $\rho_S(t)$ alone, since it depends on the state of the total system $\rho(t)$. Additional approximations are usually needed to obtain a tractable equation for the reduced dynamics [1].

2.2 Quantum master equations

Solving the full microscopic dynamics of the total system is generally impractical, since the environment contains a large number of degrees of freedom. Instead, one derives an effective equation of motion for the reduced state alone. This is the quantum master equation, which provides the framework for describing dissipation, decoherence, and relaxation in open quantum systems [1].

2.3 Markovian master equations

The Markovian approximation is justified when the bath correlation time τ_B is much shorter than the relaxation time τ_R of the open system. If the condition

$$\tau_B \ll \tau_R \tag{31}$$

is satisfied, the environmental correlations decay before they can influence the future evolution of the system, and the reduced dynamics becomes memoryless. Therefore, the future evolution depends only on the present state of the system. One also typically assumes weak system-environment coupling [1].

The reduced dynamics then become local in time and can be described by a Markovian master equation. In the time-homogeneous case, this equation takes the form

$$\frac{d\rho_S(t)}{dt} = \mathcal{L}\rho_S(t), \tag{32}$$

where $\mathcal{L}$ is the generator of the reduced dynamics. For a quantum dynamical semigroup, the generator can be written in the Lindblad form

$$\frac{d\rho_S(t)}{dt} = -\frac{i}{\hbar}[H, \rho_S(t)] + \sum_k \gamma_k \left(L_k \rho_S(t) L_k^\dagger - \frac{1}{2} \left\{ L_k^\dagger L_k, \rho_S(t) \right\} \right), \tag{33}$$

where H is an effective Hamiltonian of the system, L_k are operators describing the different dissipative channels, and γ_k are the corresponding decay rates. The first term generates coherent unitary evolution, recovering the Liouville-von Neumann equation (24) when the additional dissipative terms are absent [1, 7].

Let $V(t)$ denote the dynamical map taking the initial reduced state $\rho_S(0)$ to the state $\rho_S(t)$. The map must preserve the basic properties of a density operator. In particular, it must preserve the trace and map positive operators to positive operators

$$\rho_S \geq 0 \quad \Longrightarrow \quad V(\rho_S) \geq 0. \tag{34}$$

This property is called positivity and ensures that the evolved state yields nonnegative probabilities for all measurement outcomes. Dynamical maps $V(t)$ generate a one-parameter semigroup

$$V(t_1)V(t_2) = V(t_1 + t_2), \qquad V(0) = I. \tag{35}$$

This semigroup property expresses the Markov character of the evolution. Under suitable mathematical conditions, there exists a generator $\mathcal{L}$ such that

$$V(t) = e^{\mathcal{L}t}. \tag{36}$$

so the Lindblad equation is precisely the differential form of a quantum dynamical semigroup [7].

Beyond the Markovian regime, the generator becomes time-dependent, and the decay rates may turn temporarily negative. This is the signature of non-Markovian memory effects [2].

2.4 Positivity and complete positivity

Having introduced the master equation for the reduced dynamics, one must still require that the corresponding dynamical map is physically admissible. For open quantum systems, positivity alone is not sufficient. If the system is entangled with another system that does not take part in the evolution, the positivity of $V(t)$ on the system alone does not guarantee a physical outcome on the enlarged state. The map must therefore remain positive under extension to any auxiliary system. Thus $V(t)$ is called completely positive if

$$(V(t) \otimes I_n)(\varrho) \geq 0 \tag{37}$$

for every positive integer n and for every positive operator ϱ on the enlarged Hilbert space $\mathcal{H}_S \otimes \mathbb{C}^n$, where I_n denotes the identity map on the ancilla. Complete positivity is therefore a stronger condition than just positivity [8, 9].

This distinction is also important when one considers the evolution between intermediate times. If the inverse of the dynamical map exists, one can define the intermediate map

$$V(t,s) = V(t)V^{-1}(s), \qquad t \geq s \geq 0, \tag{38}$$

so that

$$V(t) = V(t,s)V(s). \tag{39}$$

where $V(t,s)$ describes the intermediate evolution from time s to time t. The evolution is called P-divisible if the intermediate map $V(t,s)$ is positive for all $t \geq s \geq 0$, and CP-divisible if $V(t,s)$ is completely positive for all $t \geq s \geq 0$ [2, 10].

Divisibility is directly connected to two widely used measures of non-Markovianity. The so-called BLP criterion identifies non-Markovian behavior through a temporary increase in the trace distance. The trace distance between two states ρ_1 and ρ_2 is defined as

$$D(\rho_1, \rho_2) = \frac{1}{2}\mathrm{Tr}\left|\rho_1 - \rho_2\right|, \tag{40}$$

where $|A| = \sqrt{A^\dagger A}$. Since the trace distance measures the distinguishability of quantum states and is contractive under completely positive maps, a temporary increase in $D\big(V(t)\rho_1, V(t)\rho_2\big)$ can be interpreted as a backflow of information from the environment to the system and therefore signals non-Markovian behavior. The RHP criterion instead identifies non-Markovianity with a breakdown of CP-divisibility, which can equivalently be witnessed by a temporary increase of entanglement between the open system and an isolated ancilla.The two criteria therefore characterize different aspects of non-Markovian behavior: the BLP approach through information flow, and the RHP approach through the divisibility structure of the dynamical map [11, 12].

2.5 Pure dephasing dynamics

In pure dephasing, phase coherence is lost without any change in the level populations. In the eigenbasis of the system Hamiltonian, the diagonal elements of the density matrix remain fixed while the off-diagonal elements decay in time [1, 13].

A standard time-local model of pure dephasing for a qubit is

$$\frac{d\rho}{dt} = -\frac{i}{\hbar}[H, \rho] + \gamma_z(t)\big(\sigma_z \rho \sigma_z - \rho\big), \tag{41}$$

where $H = \frac{\hbar\omega_0}{2}\sigma_z$ is the system Hamiltonian and $\gamma_z(t)$ is the time-dependent dephasing rate. The evolution is governed by a single time-dependent decoherence channel. Therefore, the notions of P-divisibility and CP-divisibility are equivalent, and both hold if and only if $\gamma_z(t) \geq 0$ [2, 14].

More generally, pure dephasing occurs when the interaction Hamiltonian commutes with the system Hamiltonian, so that the interaction is diagonal in the energy eigenbasis and cannot drive transitions between levels. A standard microscopic model is the pure-dephasing spin-boson model

$$H = H_S + H_B + H_{\text{int}}, \tag{42}$$

$$H_S = \frac{\hbar\omega_0}{2}\sigma_z, \tag{43}$$

$$H_B = \sum_k \hbar\omega_k b_k^\dagger b_k, \tag{44}$$

$$H_{\text{int}} = \sigma_z \sum_k \left(g_k b_k + g_k^* b_k^\dagger\right), \tag{45}$$

where $b_k^\dagger$ and b_k are bosonic creation and annihilation operators and g_k are coupling constants. Since $[H_S, H_{\text{int}}] = 0$, the interaction does not change the level populations and leads only to dephasing. Dephasing can also be modeled through stochastic fluctuations of the level splitting [1, 14].

Solving the master equation in the eigenbasis of σ_z, the populations are

$$\rho_{00}(t) = \rho_{00}(0) \tag{46}$$

$$\rho_{11}(t) = \rho_{11}(0), \tag{47}$$

while the coherences evolve as

$$\rho_{01}(t) = \rho_{01}(0)e^{-i\omega_0 t - 2\int_0^t \gamma_z(\tau)\,d\tau} \tag{48}$$

$$\rho_{10}(t) = \rho_{10}(0)e^{i\omega_0 t - 2\int_0^t \gamma_z(\tau)\,d\tau}. \tag{49}$$

Superpositions are therefore destroyed while the populations remain unchanged. In the Markovian case, where $\gamma_z(t) = \gamma_z$, the decay reduces to the simple exponential factor $e^{-i\omega_0 t - 2\gamma_z t}$ [2, 13].

2.6 Pauli master equation dynamics

The Pauli master equation is a time-local master equation for a qubit in which the jump operators are the Pauli matrices

$$\frac{d\rho(t)}{dt} = \frac{1}{2}\sum_{k=1}^{3} \gamma_k(t)\left(\sigma_k \rho(t) \sigma_k - \rho(t)\right), \tag{50}$$

where $\sigma_1 = \sigma_x$, $\sigma_2 = \sigma_y$, and $\sigma_3 = \sigma_z$. The coefficients $\gamma_k(t)$ are real time-dependent rates that control the strength of the three dissipative channels. Non-negative rates correspond to CP-divisible Markovian evolution, whereas temporarily negative rates indicate non-Markovian behavior [10].

When all rates satisfy $\gamma_k(t) \geq 0$, the dynamics is CP-divisible. P-divisibility is weaker, requiring only

$$\gamma_i(t) + \gamma_j(t) \geq 0, \qquad i \neq j. \tag{51}$$

so temporarily negative rates therefore do not necessarily mean that the dynamics are unphysical [10, 15].

3 Stochastic Quantum Trajectories

The dynamics described by a master equation can often be represented as an ensemble of stochastic pure-state realizations. This representation is called an unraveling

of the master equation. Unravelings offer both a trajectory-level picture of the dynamics and a numerically efficient alternative to directly evolving the full density matrix. The reduced density operator is recovered as the ensemble average

$$\rho_S(t) = \mathbb{E}[|\psi(t)\rangle\langle\psi(t)|]\,, \tag{52}$$

where $\mathbb{E}$ denotes the average over stochastic realizations. In the quantum-jump picture, each realization evolves deterministically between randomly occurring jumps [1, 3].

For Markovian master equations with non-negative rates, the unravelings are constructed by the Monte Carlo wave-function method. The jump probabilities are determined by the rates and jump operators appearing in the master equation [16].

In the non-Markovian regime, the construction of quantum-jump trajectories becomes more subtle. Time-dependent rates become temporarily negative, and this affects how the stochastic unraveling can be constructed and interpreted. The connection between quantum jumps and non-Markovianity is therefore related to the divisibility properties of the dynamical map [3, 17].

Quantum-jump unravelings are not the only possible stochastic description. Diffusive unravelings also exist, where the stochastic state changes continuously rather than through sudden jumps [4].

3.1 Quantum jump unravelings and stochastic evolution

In the quantum-jump unraveling of the Lindblad equation (33), each realization consists of deterministic evolution interrupted by random jumps. The continuous part of the evolution is generated by the effective non-Hermitian Hamiltonian

$$K = H - \frac{i\hbar}{2}\sum_k \gamma_k L_k^\dagger L_k, \tag{53}$$

where H is the system Hamiltonian, L_k are the Lindblad operators, and γ_k are the decay rates. Starting from a normalized state $|\psi(t)\rangle$ at time t, the unnormalized

no-jump state after a short time interval δt is

$$|\tilde{\psi}_0(t+\delta t)\rangle = \left(1 - \frac{i}{\hbar} K \delta t\right) |\psi(t)\rangle. \tag{54}$$

Since K is non-Hermitian, the norm of the state decreases during this evolution. This loss of norm determines the jump probability [16].

A jump in channel k occurs during the interval δt with probability

$$p_k(t) = \delta t \, \gamma_k \langle \psi(t)| L_k^\dagger L_k |\psi(t)\rangle, \tag{55}$$

after which the state is

$$|\psi(t)\rangle \longrightarrow |\psi(t+\delta t)\rangle = \frac{L_k|\psi(t)\rangle}{\sqrt{\langle \psi(t)| L_k^\dagger L_k |\psi(t)\rangle}}. \tag{56}$$

If no jump occurs, the state is renormalized

$$|\psi_0(t+\delta t)\rangle = \frac{\left(1 - \frac{i}{\hbar} K \delta t\right) |\psi(t)\rangle}{\left\| \left(1 - \frac{i}{\hbar} K \delta t\right) |\psi(t)\rangle \right\|}. \tag{57}$$

Averaging over realizations recovers the reduced density operator as in Eq. (52) [1, 16].

The Monte Carlo wave-function method applies when the decay rates remain nonnegative. In the non-Markovian regime, master equations may contain time-dependent rates that become temporarily negative, so that the standard jump interpretation can no longer be applied directly [17].

3.2 Rate operator formalism

The rate-operator formalism extends the standard quantum-jump picture beyond the regime where all decay rates are nonnegative. In the Monte Carlo method, jump probabilities are fixed directly by the rates and operators in the master equation, which fails when rates turn negative [3, 4].

The jump part of the master equation is

$$J_t[\rho] = \sum_\alpha \gamma_\alpha(t) L_\alpha(t) \rho L_\alpha^\dagger(t), \tag{58}$$

and for a normalized state $|\psi(t)\rangle$ with projector

$$P_\psi(t) = |\psi(t)\rangle\langle\psi(t)| \tag{59}$$

the rate operator is defined

$$W_\psi(t) = (I - P_\psi(t))\, J_t[P_\psi(t)]\, (I - P_\psi(t))\,. \tag{60}$$

For P-divisible dynamics, $W_\psi(t)$ is positive semidefinite. Its eigenvalues are then nonnegative and determine the jump probabilities, while its eigenvectors determine the corresponding post-jump states. The spectral decomposition can be written as

$$W_\psi(t) = \sum_j \lambda_{\psi,j}(t)|\phi_{\psi,j}(t)\rangle\langle\phi_{\psi,j}(t)|. \tag{61}$$

The jump

$$|\psi(t)\rangle \longrightarrow |\phi_{\psi,j}(t)\rangle \tag{62}$$

occurs with probability

$$p_j(t) = \lambda_{\psi,j}(t)\, dt. \tag{63}$$

The operators $L_\alpha(t)$ and rates $\gamma_\alpha(t)$ thus enter only through $W_\psi(t)$, rather than determining the jumps directly as in the Monte Carlo method [3, 4].

The decomposition of the master equation into jump and deterministic parts is not unique. For an arbitrary time-dependent operator $C(t)$, one can define a transformed jump term

$$J'_t[\rho] = J_t[\rho] + \frac{1}{2}\left(C(t)\rho + \rho C^\dagger(t)\right), \tag{64}$$

with a corresponding transformation of the deterministic part, leaving the full master equation unchanged. This leads to the transformed rate operator

$$R^C_\psi(t) = J'_t[P_\psi(t)] = J_t[P_\psi(t)] + \frac{1}{2}\left(C(t)P_\psi(t) + P_\psi(t)C^\dagger(t)\right). \tag{65}$$

where $C(t)$ is the same for all stochastic realizations. When $R_\psi^C(t)$ is positive semidefinite, its eigenvalues and eigenvectors define the jump probabilities and post-jump states. Different choices of $C(t)$ therefore yield different unravelings of the same master equation [4, 18].

3.3 Realization-dependent transformations

The state-independent transformation of the previous section can be extended by allowing $C_\psi(t)$ to depend on the current stochastic realization. The generalized rate operator then takes the form

$$R_\psi(t) = J_t[P_\psi(t)] + \frac{1}{2}\left(C_\psi(t)P_\psi(t) + P_\psi(t)C_\psi^\dagger(t)\right), \tag{66}$$

and the corresponding deterministic evolution is generated by the state-dependent non-Hermitian Hamiltonian

$$K_\psi(t) = H(t) - \frac{i}{2}\Gamma(t) - \frac{i}{2}C_\psi(t), \tag{67}$$

where $\Gamma(t) = \sum_\alpha \gamma_\alpha(t)L_\alpha^\dagger(t)L_\alpha(t)$. The dependence on the current realization makes the deterministic part of the dynamics nonlinear [4].

Since $C_\psi(t)$ appears only through its action on $|\psi(t)\rangle$, it is convenient to define the unnormalized vector

$$|\Phi_\psi(t)\rangle = C_\psi(t)|\psi(t)\rangle. \tag{68}$$

in terms of which the rate operator reads

$$R_\psi(t) = \sum_\alpha \gamma_\alpha(t)L_\alpha(t)P_\psi(t)L_\alpha^\dagger(t) + \frac{1}{2}\left(|\Phi_\psi(t)\rangle\langle\psi(t)| + |\psi(t)\rangle\langle\Phi_\psi(t)|\right). \tag{69}$$

Compared with the state-independent transformation, the additional freedom to let $|\Phi_\psi(t)\rangle$ depend on the current stochastic realization gives greater control over the stochastic trajectories, and makes it possible to construct unravelings for some non-P-divisible dynamics [4].

4 Deterministic steering of quantum trajectories in the generalized rate operator formalism

The central question is whether the realization-dependent transformation can actually be used to steer the deterministic part of individual stochastic trajectories. This is motivated by a broader and practically relevant problem of how to drive a quantum system toward a prescribed target state. Applications include state initialization, resetting protocols, and preparing resource states for quantum technologies. The goal here is not to build a full state-preparation protocol, but to use a fixed target state as a concrete way to test how much control the transformation gives over the trajectory level.

The realization-dependent transformation enters directly through the effective non-Hermitian Hamiltonian, so different choices of the transformation immediately change how the deterministic part of the evolution behaves. The main constraint is that the generalized rate operator has to stay positive semidefinite, since its eigenvalues play the role of jump probabilities and cannot be negative. The set of states where this condition holds defines the positivity domain, which for a qubit has a natural geometric picture on the Bloch sphere [4].

4.1 Overlap ratio and attraction

For a fixed realization-dependent transformation, the overlap ratio measures whether the deterministic evolution moves the current state $|\psi(t)\rangle$ toward the reference direction

$$|\tilde{\Phi}_\psi(t)\rangle = \frac{|\Phi_\psi(t)\rangle}{\sqrt{\langle\Phi_\psi(t)|\Phi_\psi(t)\rangle}}. \tag{70}$$

.

If $|\psi(t+\delta t)\rangle$ is the state after one deterministic step, the overlap ratio is defined

as

$$r(t) = \frac{|\langle\psi(t+\delta t)|\tilde{\Phi}_\psi(t)\rangle|^2}{|\langle\psi(t)|\tilde{\Phi}_\psi(t)\rangle|^2}. \tag{71}$$

When $r(t) > 1$, the deterministic evolution is locally attractive toward $|\tilde{\Phi}_\psi(t)\rangle$, when $r(t) < 1$ it is repulsive, and $r(t) = 1$ means the overlap is unchanged to first order in δt. Since only terms up to first order in δt are retained, $r(t) > 1$ signals local attraction during a single short step and does not imply long-time convergence.

Attraction alone is not sufficient for a valid unraveling. The generalized rate operator must also remain positive semidefinite, so the central question is whether both conditions can be satisfied simultaneously.

4.2 Pure dephasing dynamics

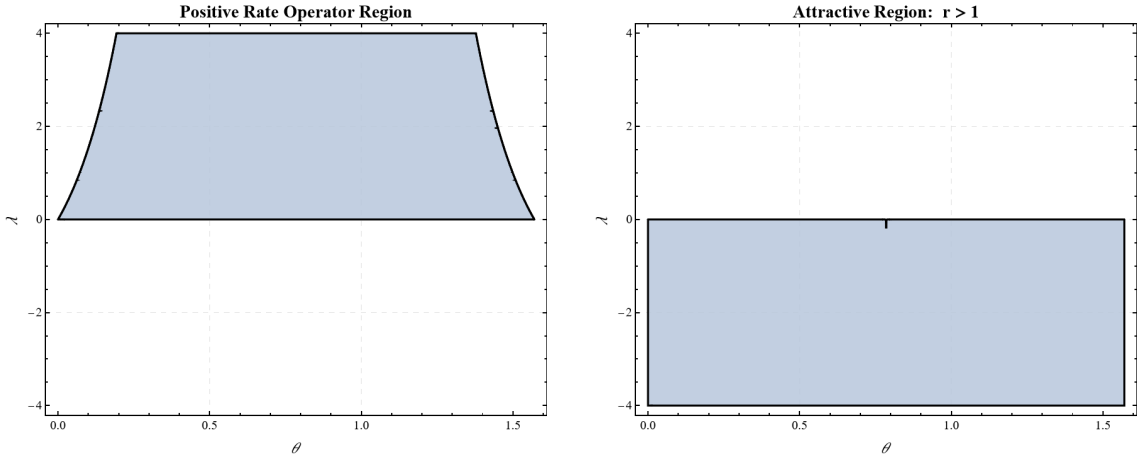

Figure 2. Parameter regions for the fixed-direction transformation in the pure dephasing case. The left panel shows where the rate operator remains positive, while the right panel shows where the overlap ratio satisfies $r > 1$. The regions do not overlap, so positivity and attraction are not obtained simultaneously for this ansatz.

The pure dephasing case serves as a concrete test of whether a simple transformation vector can produce local attraction while keeping the rate operator positive. The dephasing rate is

$$\gamma_z(t) > 0. \tag{72}$$

giving the master equation

$$\frac{d\rho}{dt} = \gamma_z(t)\left(\sigma_z\rho\sigma_z - \rho\right). \tag{73}$$

Pure states are parametrized as

$$|\psi(\theta)\rangle = \cos\theta|0\rangle + \sin\theta|1\rangle, \tag{74}$$

where $0 \leq \theta \leq \frac{\pi}{2}$. The transformation vector is fixed in the direction

$$|\Phi_\psi\rangle = \lambda|+\rangle, \tag{75}$$

where $\lambda \in \mathbb{R}$ and $|+\rangle = \frac{|0\rangle+|1\rangle}{\sqrt{2}}$.

The generalized rate operator is then

$$R_\psi = \gamma_z(t)\sigma_z P_\psi \sigma_z + \frac{1}{2}\left(|\Phi_\psi\rangle\langle\psi| + |\psi\rangle\langle\Phi_\psi|\right). \tag{76}$$

The positivity of the rate operator is checked via the smallest eigenvalue

$$\lambda_{\min}(R_\psi) \geq 0. \tag{77}$$

The effective Hamiltonian is

$$K_\psi = -\frac{i}{2}\left(\gamma_z(t)I + |\Phi_\psi\rangle\langle\psi|\right). \tag{78}$$

so the unnormalized no-jump state after one step is

$$|\psi_{\text{det}}^{\text{raw}}(t+\delta t)\rangle = \left(1 - \frac{\gamma_z(t)\delta t}{2}\right)|\psi(t)\rangle - \frac{\delta t}{2}|\Phi_\psi\rangle. \tag{79}$$

The overlap ratio is evaluated between the normalized version of this state and normalized transformation state

$$r(\theta,\lambda) = \frac{|\langle\psi_{\text{det}}(t+\delta t)|\widetilde{\Phi}_\psi\rangle|^2}{|\langle\psi(t)|\widetilde{\Phi}_\psi\rangle|^2}, \tag{80}$$

where $|\psi_{\text{det}}(t+\delta t)\rangle$ denotes the normalized deterministic state obtained from $|\psi_{\text{det}}^{\text{raw}}(t+\delta t)\rangle$. The deterministic evolution is attractive when

$$r(\theta,\lambda) > 1. \tag{81}$$

A numerical simulation was run for $\gamma_z(t) = 1$ and $\delta t = 0.01$, but the sign conflict seen in the results is not specific to these values. These parameters are representative choices only, and the same qualitative conflict appears for arbitrary positive $\gamma_z(t)$. Figure 2 shows that the positivity and attraction conditions are not satisfied in the same parameter region. The rate operator remains positive primarily for $\lambda > 0$, while attraction toward $|+\rangle$ requires $\lambda < 0$. The origin of this conflict is the deterministic correction term

$$-\frac{\delta t}{2}\lambda|+\rangle. \tag{82}$$

For $\lambda < 0$, this adds a component in the $|+\rangle$ direction, increasing the overlap with the reference state, but simultaneously pushes R_ψ outside the positivity domain. For $\lambda > 0$ the rate operator can remain positive, but the correction points away from $|+\rangle$ and produces no attraction. The fixed-direction ansatz $|\Phi_\psi\rangle = \lambda|+\rangle$ is therefore too restrictive: simultaneous positivity and attraction cannot be achieved for this test case.

4.3 Pauli master equation dynamics

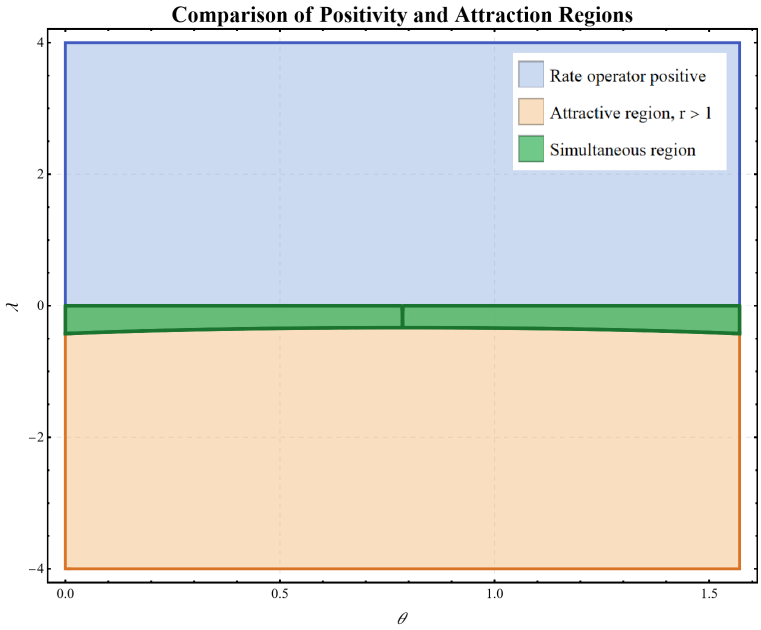

Figure 3. Parameter regions for the fixed-direction transformation in Pauli master equation dynamics, where $-4\gamma \leq \lambda \leq 4\gamma$. The figure compares the positivity of the generalized rate operator with the attraction condition $r > 1$ in the (θ, λ) plane. The blue region shows where the generalized rate operator is positive, the orange region shows where the deterministic step is attractive with $r > 1$, and the green region shows where both conditions are satisfied simultaneously.

The Pauli master equation is used as a second paradigmatic model for the generalized rate operator construction. In contrast to the pure dephasing case, the dynamics contains all three Pauli channels

$$\gamma_x(t) = \gamma_y(t) = \gamma_z(t) = \frac{\gamma(t)}{3}, \qquad \gamma > 0, \tag{83}$$

and when $H = 0$, the master equation is

$$\frac{d\rho}{dt} = \frac{\gamma(t)}{3} \sum_{k=1}^{3} \left(\sigma_k \rho \sigma_k - \rho\right), \tag{84}$$

where $\sigma_1 = \sigma_x$, $\sigma_2 = \sigma_y$, and $\sigma_3 = \sigma_z$.

The generalized rate operator is

$$R_\psi = \frac{\gamma(t)}{3} \sum_{k=1}^{3} \sigma_k P_\psi \sigma_k + \frac{1}{2} \left(|\Phi_\psi\rangle\langle\psi| + |\psi\rangle\langle\Phi_\psi|\right), \tag{85}$$

and the positivity condition is checked at every time step from the smallest eigenvalue,

$$\lambda_{\min}(R_\psi) \geq 0. \tag{86}$$

The jump part of the generalized rate operator is

$$J[\rho] = \frac{\gamma(t)}{3} \sum_{k=1}^{3} \sigma_k \rho \sigma_k. \tag{87}$$

Since

$$\sum_{k=1}^{3} \frac{\gamma(t)}{3} \sigma_k^\dagger \sigma_k = \gamma(t) I, \tag{88}$$

the deterministic part is generated by

$$K_\psi = -\frac{i}{2} \left(\gamma(t) I + |\Phi_\psi\rangle\langle\psi| \right). \tag{89}$$

For a normalized state, the unnormalized deterministic state after one time step is therefore

$$|\psi_{\text{det}}^{\text{raw}}(t+\delta t)\rangle = \left(1 - \frac{\gamma(t)\delta t}{2}\right) |\psi(t)\rangle - \frac{\delta t}{2} |\Phi_\psi\rangle. \tag{90}$$

The normalized deterministic state is then used to evaluate the overlap with the target state $|+\rangle$.

Unlike in the case of pure dephasing dynamics, the rate operator can stay positive and the overlap ratio attractive $r > 1$ simultaneously. For the positivity and attraction check, the same transformation ansatz Eq. (74) and state Eq. (75) were used. The numerical parameters are set as

$$\gamma(t) = 1, \qquad \delta t = 0.01, \qquad -4\gamma \leq \lambda \leq 4\gamma. \tag{91}$$

For each parameter pair (θ, λ) defining the state in Eq. (74) and the transformation in Eq. (75), the smallest eigenvalue of R_ψ is used to test positivity. The attraction condition is tested with the overlap ratio. The result is shown in Figure 3. Unlike

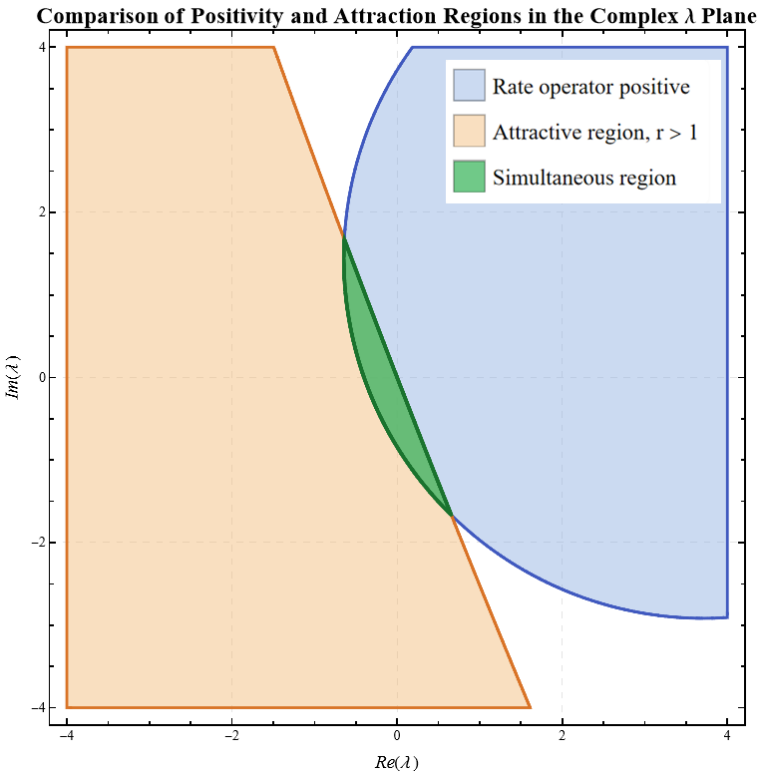

Figure 4. Parameter regions in $\lambda \in \mathbb{C}$ for Pauli master equation dynamics with $\theta = \pi/6$ and $\chi = \pi/3$. The blue region shows where the generalized rate operator is positive, the orange region shows where the deterministic step is attractive with $r > 1$, and the green region shows the overlap where both conditions hold simultaneously.

in the pure dephasing case, the Pauli master equation has a nonempty region where the generalized rate operator is positive and the deterministic step is attractive at the same time.

To check whether the coexistence of positivity and deterministic attraction is restricted to real transformation parameters, the analysis is next extended to the complex λ plane. Now the state is parametrized as

$$|\psi(\theta, \chi)\rangle = \cos\theta\,|0\rangle + e^{i\chi}\sin\theta\,|1\rangle, \tag{92}$$

where $\chi \in \mathbb{R}$ is a phase parameter. The transformation is the same as in Eq. (75), but the parameter λ is allowed to take complex values

$$\lambda \in \mathbb{C}, \qquad \lambda = \Re(\lambda) + i\,\Im(\lambda). \tag{93}$$

The same parameter values as in Eq. (91) are used, with the fixed state parameters chosen as

$$\theta = \frac{\pi}{6} \qquad \chi = \frac{\pi}{3}, \tag{94}$$

which give unequal populations and a nonzero relative phase. These values are used as a representative nontrivial state, avoiding the cases of basis states and real superposition states. The overlap between the positivity region and the attraction region in the complex λ plane is shown in Figure 4. This overlap corresponds to the parameter regime where the rate operator remains positive while the dynamics is simultaneously attractive.

The central result is that, for the Pauli master equation, positivity of the rate operator and attractive deterministic evolution can hold simultaneously. This contrasts with the pure dephasing case, where the same transformation ansatz did not produce an overlap between the positivity and attraction regions. For real values of λ, the overlap region in Figure 3 already demonstrates that the attractive behavior is compatible with positivity of the rate operator. Extending the analysis to complex λ and including a relative phase χ in the state parametrization shows that the

coexistence of the two conditions still holds. The relative phase reshapes the overlap region in a nontrivial way, as shown in Figure 4. The precise dependence on χ is beyond the scope of this thesis.

Although the numerical simulation is carried out for the target state $|+\rangle$, this choice does not represent a physically preferred direction of the isotropic Pauli dynamics. The master equation is rotationally symmetric on the Bloch sphere. Choosing $|+\rangle$ as the target is therefore no different from choosing any other pure state. This observation is relevant from the perspective of state preparation. If the chosen target is replaced by $|0\rangle$, the same symmetry argument connects the present steering problem to ground-state preparation, where dissipation can be used to drive a system toward a desired stationary or low-energy state [5].

4.3.1 Simulation of deterministic attraction

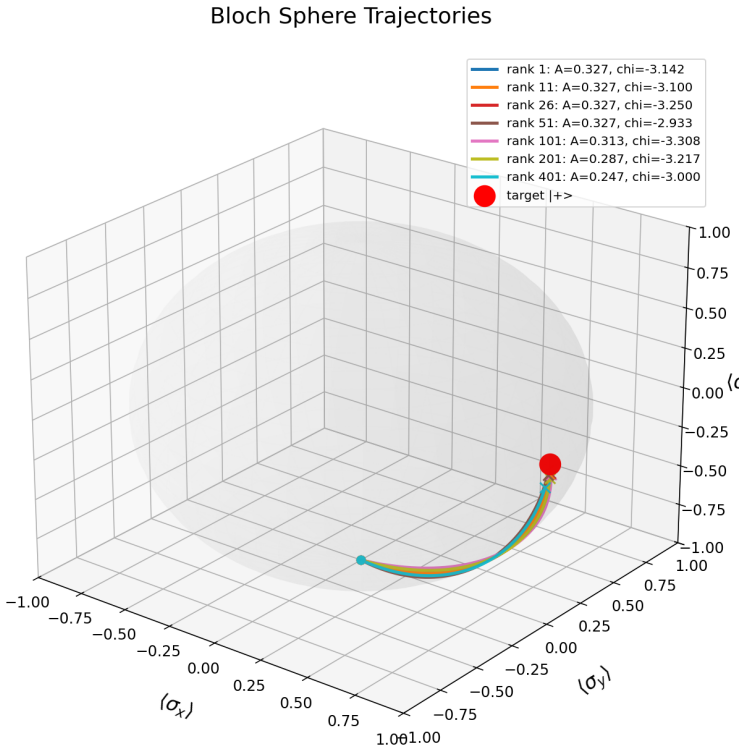

Figure 5. Bloch-sphere representation of deterministic trajectories for several accepted fixed transformations. Each coloured curve corresponds to a different parameter pair (A, χ). The red marker denotes the target state $|+\rangle$. All shown trajectories satisfy the positivity condition. The parameter pairs are ranked according to their integrated survival probability.

The idea is to study how the realization-dependent transformation affects the deterministic part of the unraveling. Pure states are parametrized on the Bloch sphere as

$$|\psi(\theta, \varphi)\rangle = \cos\theta|0\rangle + e^{i\varphi}\sin\theta|1\rangle, \tag{95}$$

where $0 \leq \theta \leq \frac{\pi}{2}$ and $0 \leq \varphi < 2\pi$. The transformation vector is chosen as

$$|\Phi_\psi\rangle = Ae^{i\chi}|+\rangle, \tag{96}$$

where $A \geq 0$ is a real amplitude.

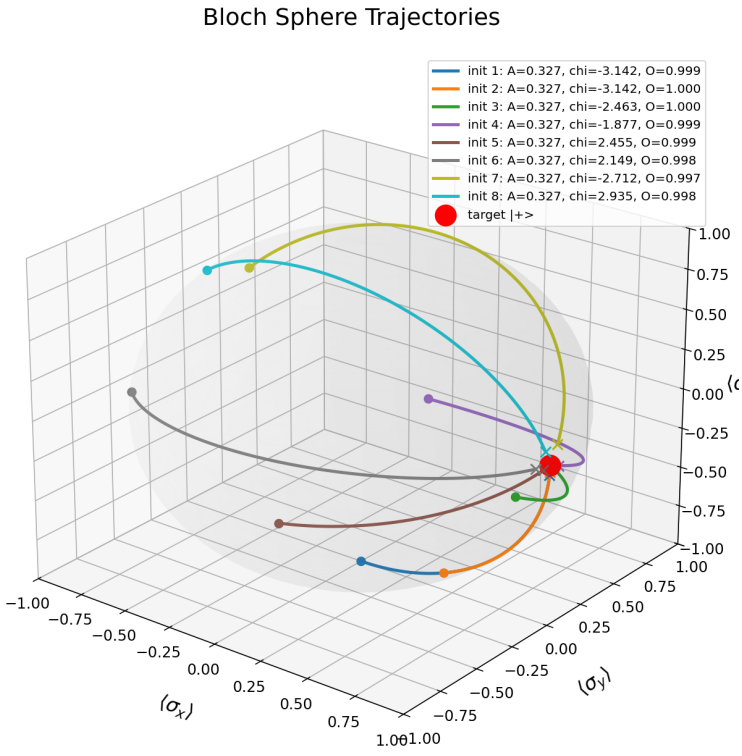

Figure 6. Bloch-sphere representation of deterministic trajectories for several different initial states. Each coloured curve corresponds to a different initial state, with its optimized parameter pair (A, χ). The red marker denotes the target state $|+\rangle$. All shown trajectories satisfy the positivity condition and reach the prescribed minimum target overlap. For each initial state, the parameter pair was selected by maximizing the integrated survival probability.

The transformation parameters A and χ are numerically sampled over the parameter range $A \in [0, 1]$ and $\chi \in [-\pi, \pi]$. For each pair (A, χ), the trajectory is propagated deterministically and the generalized rate operator is required to remain positive during the full evolution. In addition, the final overlap with the target state is required to satisfy

$$f(t_{\text{arr}}) = |\langle +|\psi(t_{\text{arr}})\rangle|^2 \geq 0.96, \tag{97}$$

where t_{arr} denotes the arrival time.

The scan was then used to find a fixed transformation that satisfies the positivity condition and drives the deterministic trajectory toward the target state. Several accepted trajectories are shown in Figure 5. Each curve corresponds to a different fixed parameter pair (A, χ), which is kept constant throughout the simulation. The red marker denotes the target state $|+\rangle$. All plotted trajectories reach the target-overlap threshold defined in Eq. (97). The same is presented in Figure 6, but with different initial states, so one can see how the transformations lead to different geometries on the Bloch Sphere.

In this simulation, the optimal parameter pair was selected with maximizing the integrated survival probability. The survival probability is

$$P_{\text{surv}}(t) = \|\psi_{\text{det}}^{\text{raw}}(t)\|^2. \tag{98}$$

Within the scanned parameter range $A \in [0, 1]$ and $\chi \in [-\pi, \pi]$ the optimal parameter pair was

$$A = 0.3267 \qquad\qquad \chi = -\pi. \tag{99}$$

The smallest eigenvalue of the generalized rate operator remained positive during the full trajectory, showing that the positivity condition was not violated.

The attraction of the deterministic trajectory was tested with the overlap ratio $r(t)$. For the optimal parameter combination, the overlap ratio remained above one

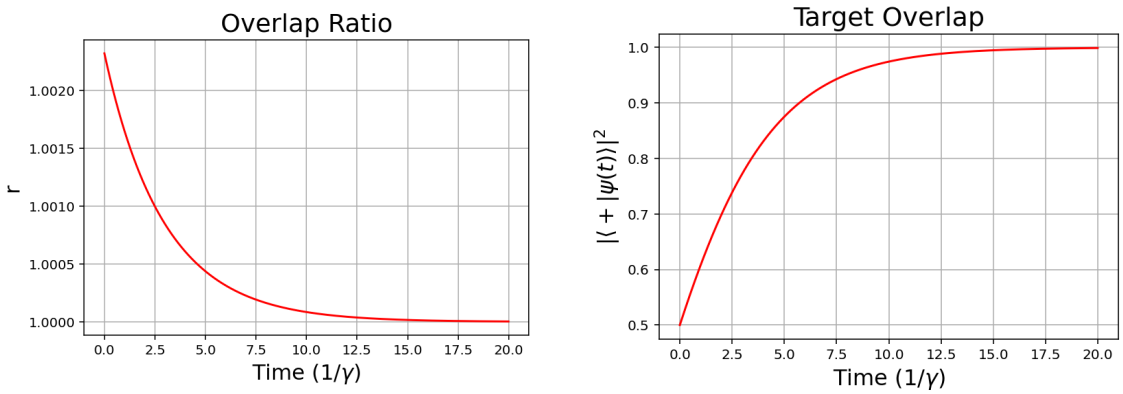

Figure 7. Overlap behaviour for the optimal parameter pair in Pauli master equation dynamics with $A = 0.3267$ and $\chi = -\pi$, $\gamma = 1$. The left panel shows the overlap ratio $r(t)$, which remains above one during the evolution and therefore indicates local attraction toward the target direction. The right panel shows the target overlap $|\langle +|\psi(t)\rangle|^2$, which increases close to one as the state approaches $|+\rangle$.

throughout the entire simulation. This confirms that each deterministic step moved the state closer to the target state and is also reflected in the target overlap, which increased from the initial value to $f(t_{\mathrm{arr}}) = 0.999$. The time evolution of both $r(t)$ and $f(t)$ is shown in Figure 7.

The generalized rate operator remains positive along the trajectory, while the deterministic evolution moves the state along the surface of the Bloch sphere toward the target state $|+\rangle$. The overlap-ratio plot confirms that the deterministic evolution is locally attractive throughout the simulation. The result therefore supports the conclusion that within the scanned range the Pauli master equation provides enough freedom for a realization-dependent transformation to improve the deterministic trajectory without violating positivity.

4.3.2 Survival probability

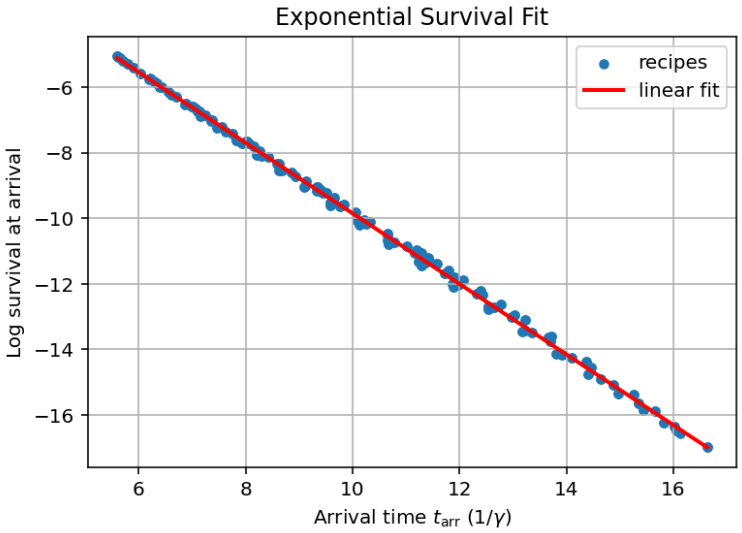

Figure 8. Logarithm of the survival probability at arrival as a function of the arrival time for the accepted fixed transformations. Each point corresponds to one fixed parameter pair (A, χ) that preserves positivity of the generalized rate operator and reaches the target-overlap threshold.

The final part of the analysis looks at how quickly different fixed transformations reach the target state and what is the asymptotic survival probability. The survival probability was tracked through the norm of the unnormalised deterministic state as in Eq. (98), which tells how much probability weight remains in the no-jump evolution up to time t. For each fixed transformation, the code checks that the generalized rate operator stays positive along the trajectory, and records the first time the target overlap crosses the threshold in Eq. (97). The corresponding value $P_{\mathrm{surv}}(t_{\mathrm{arr}})$ is then used to compare the different transformations against each other.

The simulation uses the same parameter range for A and χ as before, with $\gamma = 1$, $\delta t = 0.01$, and 2000 time steps. Only transformations that both preserved positivity and reached the target-overlap threshold were included to the comparison. To rank the accepted transformations, the simulation assigns each accepted transformation

a score

$$S = \frac{P_{\mathrm{surv}}(t_{\mathrm{arr}}) f(t_{\mathrm{arr}})}{1 + t_{\mathrm{arr}}}, \tag{100}$$

which rewards short arrival times, high survival probability, and large target overlap at arrival. The score was used to rank the accepted fixed transformations. Since each parameter pair (A, χ) defines one deterministic no-jump trajectory, this also orders the corresponding trajectories by their speed-survival performance. The numerator combines the survival probability at arrival with the target overlap, so only transformations that both reach the target reliably and retain enough no-jump probability get a high score. The denominator penalises long arrival times, meaning that even if two transformations have similar survival probabilities, the one that gets there faster is more favourable for state preparation. Large values of S therefore correspond to transformations that reach the target quickly, with high overlap and a large remaining no-jump probability. The score is used only as a numerical ordering criterion.

Figure 8 plots $\log P_{\mathrm{surv}}(t_{\mathrm{arr}})$ as a function of t_{arr} for the accepted fixed transformations. The points fall close to a straight line, which suggests the survival probability decays roughly as

$$P_{\mathrm{surv}}(t_{\mathrm{arr}}) \approx C e^{-\Gamma_{\mathrm{eff}} t_{\mathrm{arr}}}, \tag{101}$$

where C is a constant and Γ_{eff} is an effective decay rate. The fitted rate is $\Gamma_{\mathrm{eff}} \approx 1.076$, which is very close to $\gamma = 1$. This suggests that the survival probability at arrival is primarily controlled by the natural exponential decay of the no-jump evolution, while the different transformations mainly affect the arrival time to the target region.

Within the scanned parameter range, changing the transformation mainly affects the geometry and speed of the deterministic trajectory. The survival probability at arrival, on the other hand, follows roughly the same exponential dependence on t_{arr}

across all transformations. Faster transformations arrive earlier and therefore retain more no-jump probability.

The best-performing transformations came from a balance between steering strength and keeping the generalized rate operator positive. When A is too small the steering is weak and the trajectory takes a long time to reach the target. When A is too large the rate operator tends to drift outside the positivity domain. In the parameter scan phases near $\chi \approx -\pi$ were most often associated with the better-performing transformations. These findings show that the generalized rate-operator transformation gives enough freedom not only to produce an attractive no-jump trajectory toward the target state, but also to allow transformations with more favourable survival properties.

5 Conclusion

This thesis studied whether realization-dependent transformations in the generalized rate operator quantum jump formalism can be used to steer the deterministic part of individual stochastic trajectories. The motivation comes from a broader state-preparation problem. In many quantum-technology settings it is important to drive a system reliably toward a prescribed target state. Practical examples include qubit initialization and resetting in quantum computation, where the system needs to be brought to a known state before or during a computational protocol [19], and the preparation of magic states needed for universal fault-tolerant quantum computation when combined with Clifford operations [20]. In these settings the relevant question is not only whether the target state can be reached at all, but also how fast and with what probability.

The results show that the answer depends strongly on both the structure of the open-system dynamics and the choice of transformation. For pure dephasing dynamics, the fixed-direction transformation considered here did not produce simultaneous

attraction toward the target state and positivity of the generalized rate operator. This does not mean that steering is impossible for all transformations, but it does show that this particular ansatz does not give enough freedom in the pure dephasing case.

The situation was different for the Pauli master equation dynamics. Within the scanned parameter range, fixed time-independent transformations were found that kept the generalized rate operator positive while steering the deterministic trajectory toward the target state. The most optimal transformation in the scan reached a high target overlap while keeping the smallest eigenvalue of the rate operator positive throughout the full trajectory. These results indicate that, for the Pauli dynamics, the realization-dependent transformation provides enough freedom for deterministic trajectory level steering without violating the positivity condition [4].

The survival probability results gave a clearer picture of what the transformations actually do. The accepted transformations did not just differ in whether they reached the target state, they also differed in how quickly they got there and how much no-jump probability was left at arrival. Faster transformations arrive earlier and have more survival probability, while weaker transformations may stay positive but take much longer to reach the target. Across the scan, the survival probability at arrival followed roughly an exponential dependence on the arrival time, which suggests that the main effect of the transformation was to shift the arrival time rather than change the underlying decay scale of the no-jump evolution.

Overall, the results suggest that realization-dependent transformations can serve as a genuine trajectory level control mechanism. The numerical analysis provides evidence for a potentially feasible state preparation protocol in which deterministic attraction toward a chosen target state is combined with positivity preservation and survival probability optimization. The results show that the freedom provided by the generalized rate-operator formalism can be used to steer deterministic no-jump

trajectories while maintaining the positivity condition required for a valid quantum-jump interpretation. This makes the formalism a promising starting point for future work on fast and reliable preparation of desired quantum states in open quantum systems.

Use of artificial intelligence tools

The free version of ChatGPT by openAI was used as a supporting tool during the numerical part of this work. Specifically, it was consulted to help identify and understand value errors in the Python code when the errors could not be resolved independently. It was also used to support the improvement of the Mathematica plotting code, in order to improve the clarity and presentation of the plots.

References

[1] H.-P. Breuer and F. Petruccione, *The theory of open quantum systems* (Oxford University Press, 2007).

[2] H.-P. Breuer, E.-M. Laine, J. Piilo and B. Vacchini, Reviews of Modern Physics **88**, 021002 (2016).

[3] A. Smirne, M. Caiaffa and J. Piilo, Physical Review Letters **124**, 190402 (2020).

[4] F. Settimo, K. Luoma, D. Chruściński, B. Vacchini, A. Smirne and J. Piilo, Physical Review A **109**, 062201 (2024).

[5] L. E. Ballentine, *Quantum mechanics: a modern development*, repr ed. (World Scientific, 2010), p. 52.

[6] B. Schumacher and M. D. Westmoreland, *Quantum processes, systems, and information* (Cambridge University Press, 2010).

[7] R. Alicki and K. Lendi, *Quantum Dynamical Semigroups and Applications*, Vol. 717 of *Lecture Notes in Physics* (Springer Berlin Heidelberg, 2007).

[8] J. M. Dominy, A. Shabani and D. A. Lidar, Quantum Information Processing **15**, 465 (2016).

[9] F. Buscemi, Physical Review Letters **113**, 140502 (2014).

[10] M. J. W. Hall, J. D. Cresser, L. Li and E. Andersson, Physical Review A **89**, 042120 (2014).

[11] H.-P. Breuer, E.-M. Laine and J. Piilo, Physical Review Letters **103**, 210401 (2009).

[12] Á. Rivas, S. F. Huelga and M. B. Plenio, Physical Review Letters **105**, 050403 (2010).

[13] J. L. Skinner and D. Hsu, The Journal of Physical Chemistry **90**, 4931 (1986).

[14] D. Chruściński, Physics Reports **992**, 1 (2022).

[15] K. Siudzińska and D. Chruściński, Journal of Physics A: Mathematical and Theoretical **53**, 375305 (2020).

[16] J. Dalibard, Y. Castin and K. Mølmer, Phys. Rev. Lett. **68**, 580 (1992).

[17] J. Piilo, S. Maniscalco, K. Härkönen and K.-A. Suominen, Physical Review Letters **100**, 180402 (2008).

[18] D. Chruściński, K. Luoma, J. Piilo and A. Smirne, Quantum **6**, 835 (2022).

[19] J. Tuorila, M. Partanen, T. Ala-Nissila and M. Möttönen, npj Quantum Information **3**, 27 (2017).

[20] S. Bravyi and A. Kitaev, Physical Review A **71**, 022316 (2005).